Silicon (2022) 14:8581–8597
https://doi.org/10.1007/s12633-021-01652-w

ORIGINAL PAPER

Crystallization and Radiation Proficiency of Transparent Sodium Silicate Glass Doped Zirconia

E. A. Abdel Wahab[1] · Ateyyah M. Al-Baradi[2] · M. A. Sayed[1,3] · Atif Mossad Ali[3,4] · Sayed A. Makhlouf[1] · Kh. S. Shaaban[5]

Received: 25 November 2021 / Accepted: 29 December 2021 / Published online: 13 January 2022

Abstract
A sequence of transparent homogenous glasses consists of $50Na_2O$ – (50–x) SiO_2 – $xZrO_2$, ($0 \le x \le 20$ mol %), are synthesized by conventional method. All prepared samples are confirmed in an amorphous state by the X-rays diffraction XRD. The glass temperature T_g, crystallization temperature T_c, and temperature of full crystallization T_p values are increased by the increment of ZrO_2. For heat-treated glasses, the XRD results show that most selected glasses appear to be completely crystallized. ^{133}Ba, ^{137}Cs and ^{60} Co sources are used for experimental measurements of the mass attenuation coefficient (MAC) of γ-rays at 365, 662, 1172 and 1332 keV respectively and theoretical calculation were depicted using XCOM, MCNP5 and Phy-X/PSD programs procedures. MAC of our samples was compared with some commercial and published nuclear radiation shielding as ordinary concrete, 100% $Na_2B_4O_7$ and 100% SiO_2 glasses systems.

Keywords ZrO_2 · DTA · Crystallization · MAC · Effective atomic number

1 Introduction

Recently, the unique physiochemical properties and multifunctional uses of sodium silicate doped zirconate have great attention [1–8]. Because of the importance of sodium silicate glasses in science and technology, they are in continues demand for many applications like solid electrolytes in battery storage. Using transition metals (TM), also improves optical, electric, thermal, and radiation protection properties.

Glasses containing (TM) draw a lot of attention because of their advantages [9]. For different applications like windows, reflections, mechanical and thermal sensors and nuclear radiation technologies, glasses containing transition metals have gained significant attention [10–12]. In the last period, implementations study for these substances had already expanded compared to the previous period. One of the most important elements is Zr, due to its physical and chemical properties. ZrO_2 is a broadband semiconductor, which has significant interest due to its great photochromic and electrochromic features [1–8].

Radioactive technology has a strong impact and has enormous medical and industrial applications, so this technology is essential to us. Neutrons, gamma, and X-rays were widely used in numerous fields, such as food safety, protecting the environment, heavy industry, and therapeutic approaches. Even so, long-term contact with radiation, like gamma, can cause gene variations. Consequently, to protect people from such dangerous rays, it is necessary to select suitable shielding materials [13–16]. Glass has become extremely popular role, in addition to compensating for concrete defects, glass is easily performed and transparent, with a broad ions concentration range [13–16].

The sodium silicate zirconate NSZ glass has a high level of application in radiation shielding with the composition of $50Na_2O$–(50–x) SiO_2– $xZrO_2$, ($0 \le x \le 20$ mol %). The impact of ZrO_2 on lithium lead borate glasses had been studied by Abouhaswa et al., [17]. It reported that the improvement of radiation protection with the addition of ZrO_2. Few

✉ E. A. Abdel Wahab
essam.ah77@gmail.com;
essamabdelwahab1011.el@azhar.edu.eg

1 Physics Department, Faculty of Science, Al-Azhar University, P.O. Box 71524, Assiut, Egypt

2 Department of Physics, College of Science, Taif University, P.O. Box 11099, Taif 21944, Saudi Arabia

3 Physics Department, Faculty of Science, King Khalid University, Abha 61413, Saudi Arabia

4 Department of Physics, Faculty of Science, Assiut University, Assiut 71516, Egypt

5 Chemistry Department, Faculty of Science, Al-Azhar University, P.O. Box 71524, Assiut, Egypt

Table 1 Chemical composition and elements ratio of the NSZ glasses

	Element Ratio				Chemical Composition		
Sample name	Si	O	Na	Zr	SiO_2	Na_2O	ZrO_2
NSZ1	0.1667	0.5000	0.3333	0	50	50	0
NSZ2	0.1500	0.5000	0.3333	0.0167	45	50	5
NSZ3	0.1333	0.5000	0.3333	0.0333	40	50	10
NSZ4	0.1000	0.5000	0.3333	0.0667	30	50	20

experiments on ZrO_2 doped silicate glass were performed therefore, the link between both the improve in glass structure and radiation shielding has been discovered, prompting us to carry out this study.

Ceramic glasses have become indispensable materials in our daily lives due to their wide range of applications, compositional flexibility, and customizability [18–20]. ZrO_2 is an excellent nucleating agent and creates crystallization sites for nucleation. Earlier, we have studied the linear and nonlinear optical, structural, and mechanical characteristics of the NSZ glasses. The NSZ glasses were explored pioneer features as the formation of new strong bond Si–O-Zr and break the weak bond Si–O-Na with ZrO_2 concentration and the increase of ultrasonic velocities, elastic moduli, and refractive index with increasing the amounts of zirconia are obtained [21, 22]. Therefore, the goal of this article is to investigate the radiation protection features by using XCOM, MCNP-5, Phy-X/PSD programs software and crystallization characteristics of silicate glasses doped with ZrO_2.

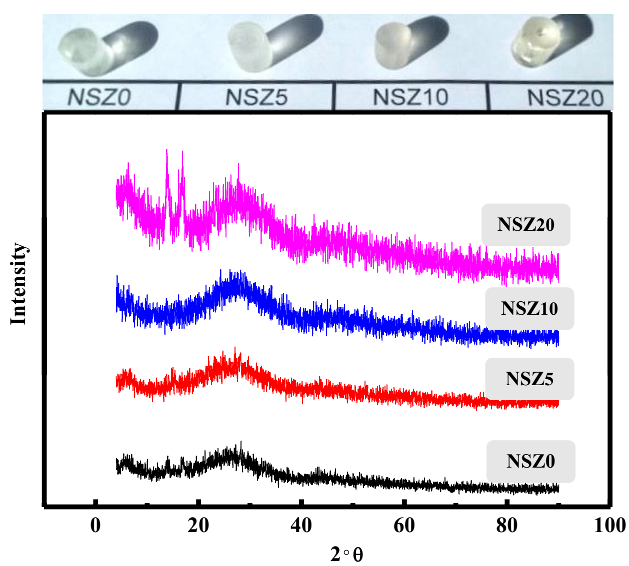

Fig. 1 The samples photo and the pattern of XRD of NSZ glasses

2 Materials and Methods

Glass samples were synthesized with the composition $50Na_2O$-(50-x) SiO_2 -xZrO_2, ($0 \leq x \leq 20$ mol %) are shown in Table 1 and ref. [21, 22]. An appropriate amount of Na_2CO_3, SiO_2, and ZrO_2 obtained from Aldrich Chemical Company was mixed and grinded in agate mortar as the start material for the present NSZ glasses. Traditional melt quenching technique was used to prepare NSZ samples at temperature 1150 °C, then left in the furnace at this temperature for two hours. The melt was stirred every half hour until the sample became completely homogeneous and then poured in the hot-plate form of discs and rods. Subsequently, the mold was transferred directly to an annealing furnace at a temperature of 375 °C to release the thermal stress, keep via gradual cooling. The thermal investigation was carried out with a DTA-50 (type Shimadzu). Then, the prepared mother glasses were heat-treated at the required temperatures according to DTA results to obtain glass–ceramic materials. Glass–ceramics are produced after 4 h at T_c °C. The XRD diffractometer was used to determine the status of these glasses and glass–ceramics.

The (MAC) mass attenuation coefficient (μ/ρ) is considered as [1]:

$$I = I_0 e^{(\frac{\mu}{\rho})x} \tag{1}$$

where I the intensity of γ – rays in the sample, I_o is the intensity of γ – rays before the sample, μ is MAC, ρ the density and x is the thickness. comparative study of XCOM Programs Phy-x/PSD and MPNC5 have been established to estimate the values of (μ/ρ) theoretically as: [23–26]:

$$(\mu/\rho) = \sum_j w_j (\mu/\rho)_j \tag{2}$$

The half-value layer (HVL) can also be applied as [1, 27, 28]:

$$HVL = \frac{ln(2)}{\mu} \tag{3}$$

Effective atomic number (Z_{eff}) and effective electron density are considered as [29–31]:

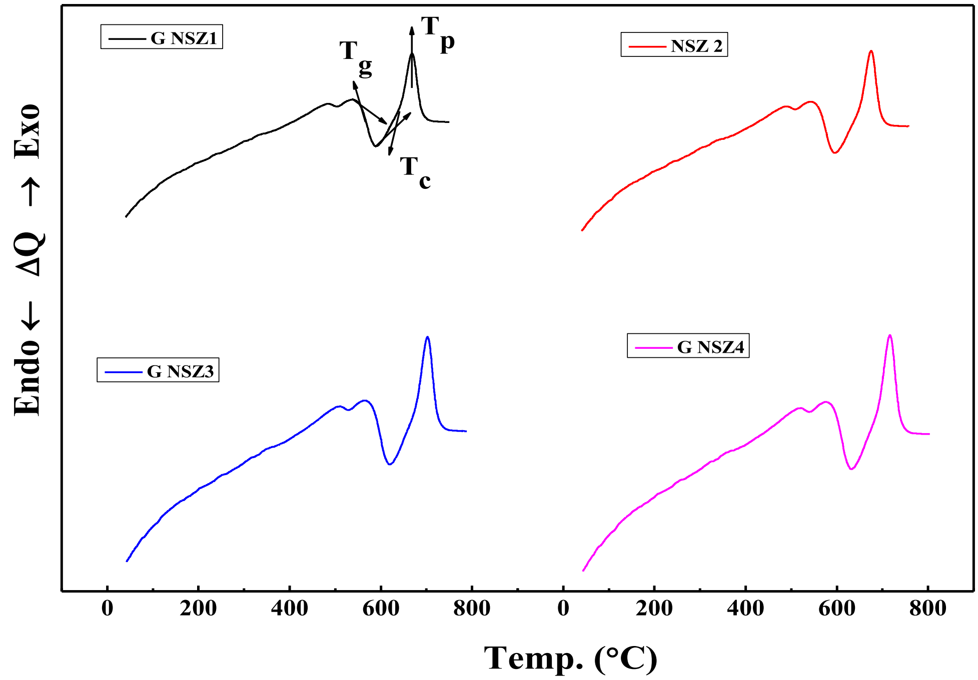

Fig. 2 DTA data of the investigated NSZ glasses

$$Z_{eff} = \frac{\sum_j f_j A_j (\frac{\mu}{\rho})_j}{\sum_j f_j (\frac{A_j}{Z_j})(\frac{\mu}{\rho})_j} \tag{4}$$

$$N_{eff} = \frac{N_A}{M} Z_{eff} \sum n_j \tag{5}$$

The equivalent atomic number (Z_{eq}) calculated from the following connection;

$$Z_{eq} = \frac{Z_1(\log R_2 - \log R) + Z_2(\log R - \log R_1)}{\log R_2 - \log R_1} \tag{6}$$

The G-P fitting is used to compute (EABF) [32, 33]:

$$C = \frac{C_1(\log Z_2 - \log Z_{eq}) + C_2(\log Z_{eq} - \log Z_1)}{\log Z_2 - \log Z_1} \tag{7}$$

$$B(E, X) = 1 + (\frac{b-1}{K-1})(K^x - 1), for K \neq 1 \tag{8}$$

$$B(E, X) = 1 + (b-1)x, for K = 1 \tag{9}$$

where:

$$K(E, x) = cx^a + d\frac{tanch\left(\frac{x}{X_K} - 2\right) - tanch(-2)}{1 - tanch(-2)} for x \leq 40 mfp \tag{10}$$

The removal cross-sections (Σ_R) of fast neutrons are predictable as [34, 35].

$$\sum R = \sum W_j (\sum \frac{R}{\rho})_j \tag{11}$$

3 Results and Discussion

3.1 DTA Analysis

For all studied compositions, the XRD patterns explored amorphous states as shown in Fig. 1 [33]. DTA was performed to characterize the thermal behavior and the thermal stability of the NSZ glasses. A trace of the DTA for glass samples is depicted in Fig. 2. The endothermic peak is demonstrated as the glass transition (T_g), then

Table 2 Thermal data analysis (DTA) values of NSZ glasses

Sample name	T_g	T_c	T_p	ΔT	H_g	T_p—Tc	S
SNZ1	544	617	668	73	0.134	51	6.84
SNZ2	551	631	679	80	0.145	48	6.97
SNZ3	573	654	703	81	0.141	49	6.93
SNZ4	587	666	719	79	0.135	53	7.1

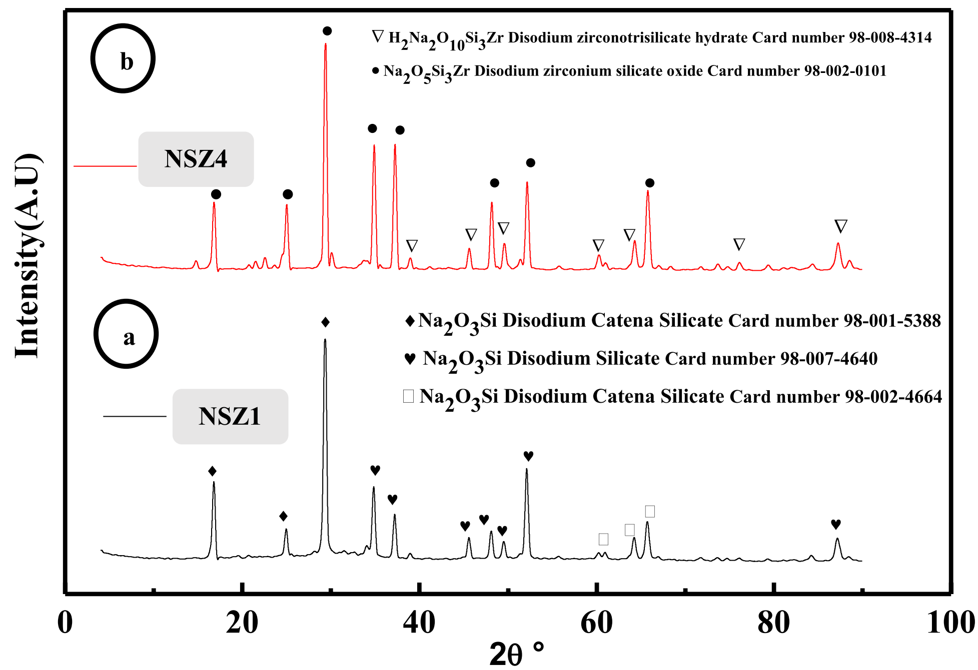

Fig. 3 XRD pattern of the selected NSZ glass–ceramic samples

exothermic two peaks are demonstrated as the initial temperature of crystallization (T_c) and full temperature of crystallization (T_p). These parameters are ascribing to the glass crystallization process. The values of T_g, T_c, and T_p, are presented in Table 2. In the present investigation, the ZrO_2 content increased at the expense of SiO_2 content this is attributed to the increase of The T_g, T_c, and T_p values for all glass compositions prepared. The interpretation of this behavior is connected by increasing the averaged force constant due to adding ZrO_2. As discussed previously [33], ZrO_2/SiO_2 replacement improves the connectivity of the glass matrix and T_g [36]. It is because of the transformation of Si – O – Na into Si – O – Zr , and Na – O bond strength is (20KCal/mol) is much lower than Zr – O (61KCal/mol) [37]. The thermal stability values as$\Delta T = \left(T_c - T_g\right)$, $Hg = \frac{\Delta T}{Tg}$, and $S = (T_p - T_c)\frac{\Delta T}{Tg}$. Table 2 shows these results.

3.2 XRD of Ceramic-Glass

As shown in Fig. 3a and b glass–ceramics of NSZ1, NSZ4 were investigated through XRD diffractometer. The XRD results for heat-treated glasses show that most glasses appear to be completely crystallized

Table 3 The XRD features of the selected glass–ceramics NSZ1

Peak number	B obs. [°2Th]	B std. [°2Th]	Peak pos. [°2Th]	B struct. [°2Th]	Crystallite size [Å]	Crystallite size [nm]	Lattice strain [%]
1	0.334	0.080	12.819	0.324	315	31.5	1.26
2	0.354	0.080	24.379	0.345	297	29.7	0.697
3	0.413	0.080	29.379	0.405	247	24.7	0.674
4	0.354	0.080	34.845	0.345	304	30.4	0.479
5	0.354	0.080	37.211	0.345	306	30.6	0.447
6	0.354	0.080	48.099	0.345	317	31.7	0.337
7	0.413	0.080	52.109	0.405	266	26.6	0.362
8	0.413	0.080	64.241	0.405	282	28.2	0.282
9	0.413	0.080	65.718	0.405	284	28.4	0.274
10	0.59	0.080	87.175	0.585	215	21.5	0.268

Table 4 The XRD features of the selected glass–ceramics NSZ4

Peak number	B obs. [°2Th]	B std. [°2Th]	Peak pos. [°2Th]	B struct. [°2Th]	Crystallite size [Å]	Crystallite size [nm]	Lattice strain [%]
1	0.354	0.080	12.840	0.274	292	29.2	1.337
2	0.354	0.080	25.039	0.274	297	29.7	0.678
3	0.413	0.080	29.404	0.333	247	24.7	0.674
4	0.413	0.080	34.899	0.333	250	25	0.562
5	0.472	0.080	37.253	0.392	214	21.4	0.602
6	0.413	0.080	45.621	0.333	259	25.9	0.420
7	0.413	0.080	48.154	0.333	261	26.1	0.396
8	0.413	0.080	49.565	0.333	263	26.3	0.383
9	0.413	0.080	52.153	0.333	266	26.6	0.361
10	0.354	0.080	64.299	0.274	342	34.2	0.239
11	0.531	0.080	65.773	0.451	210	21	0.354
12	0.472	0.080	87.270	0.392	280	28	0.213

[38–40]. As ZrO_2 increases, the intensity increases, and peak position is slightly shifted towards higher 2θ° values. High Score (Plus) v.4.0–4.8a program is used for detecting the crystallized phase in the glass–ceramic samples. The strongest phase in NSZ1 (Disodium Catena Silicate, Na_2O_3Si, card No. 98–001-5388), with a score of 73% (Sodium Silicate, Na_2O_3Si, card No. 98–002-4664), with a score of 53%, (Disodium Silicate, Na_2O_3Si, card No. 98–007-4640), with score 31%. The strongest phase in NSZ4 (Disodium zircon-trisilicate $Na_2O_9Si_3Zr$, card No. 98–008-4314) with a percentage of 45% and (Disodium zirconium silicate oxide Na_2O_5SiZr, card No. 98–002-0101) with a percentage of 55%. Some of the XRD features are shown in

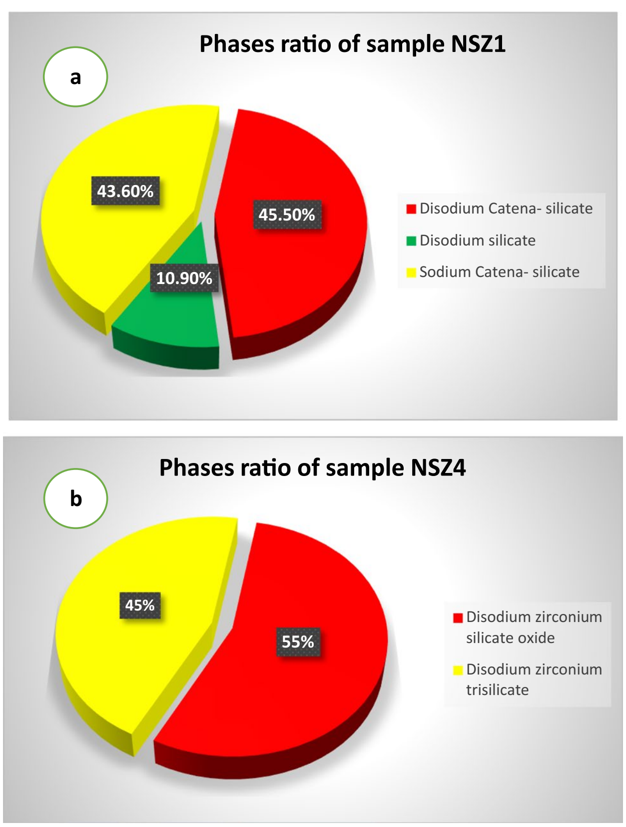

Fig. 4 Quantification diagram of the detected phases in glass–ceramic NSZ1(**a**) and NSZ4 (**b**)

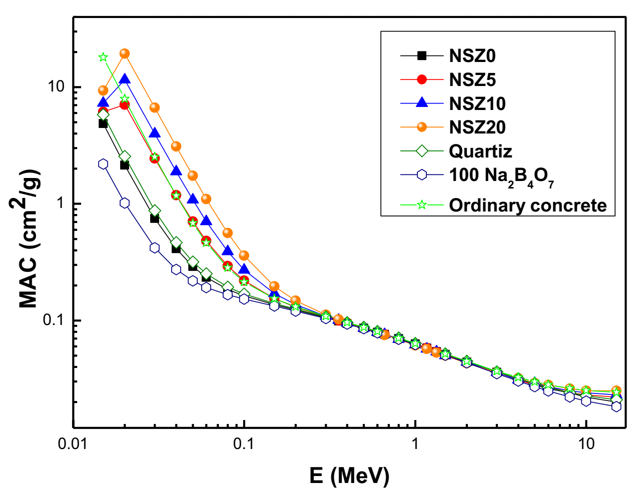

Fig. 5 Calculated MAC by using Phy-x/PSD NSZ glass compared with other glasses

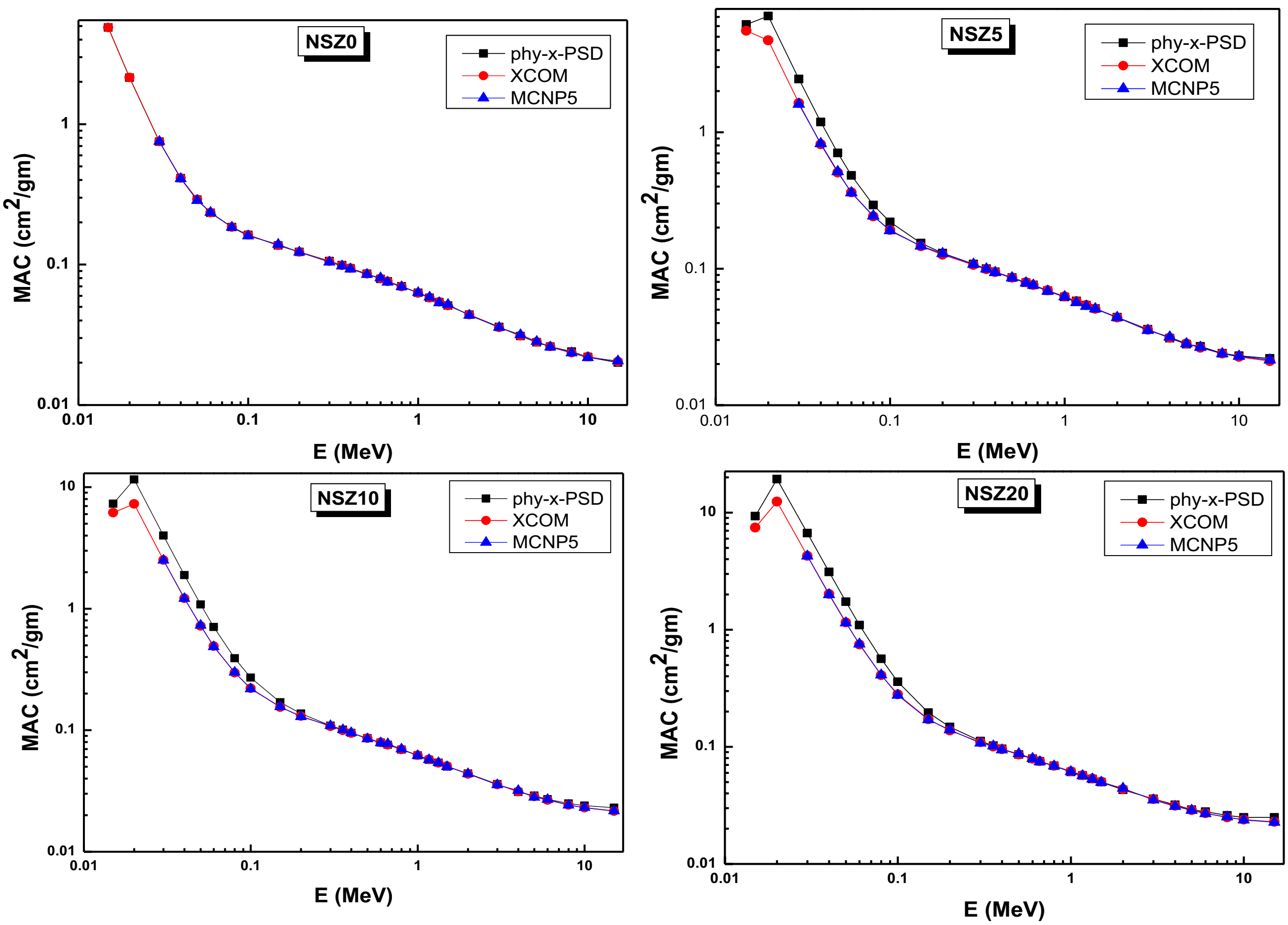

Fig. 6 Calculated MAC by different software for NSZ glasses

Tables 3 and 4. Quantification of the detected phases in the selected glass–ceramic are provided in Fig. 4a and b.

3.3 Radiation Characterization

MAC of fabricated glasses is represented in Fig. 5, the MAC value increased gradually from NSZ1 to NSZ4. This rise could be due to the replacement of a higher ZrO_2 mass portion with the lower SiO_2 molecular weight. The photoelectric effect is responsible for the rapid decline of MAC with energy. Figure 6 and Table 5 demonstrate the results of the XCOM, MCNP5, and Phy-X/PSD techniques[41]. Between the examined glass samples, the highest ZrO_2 -containing glass, unlike other glass samples, presented the highest gradient, which implies the greatest μ value. Note that the atomic number of the zirconium (Z = 40) is higher than silicon (Z = 14). Interactions between gamma and glass samples will increase when high atomic number of zirconium is added to the investigated glass samples. Due to the higher atomic number of zirconium, the further energy will be absorbed to take out electrons from the Zr atom. The electrons can be liberated by Compton scattering or photoelectric effects. As the interaction between gamma radiation and the target atom (Zr) increases, radiation transmitted through the glass decreases (Table 5). Consequently, the mass attenuation coefficient (μ/ρ) values increase. The XCOM data of MAC is better than other programs. The deviation of the results is calculated and listed in Table 5:

$$RD\% = \left(\frac{(\mu_m)_{XCOM} - (\mu_m)_{(MCNP5) or (Phy-x)}}{(\mu_m)_{XCOM}}\right) \times 100 \quad (12)$$

The variation of "linear attenuation coefficient" LAC with energy is described in Fig. 7. LAC values

Table 5 Comparison MAC calculated by different software for NSZ glass

Energy	MAC from XCOM	MAC from MCNP5	Dev% XCOM&MCNP	MAC from Phy-x/PSD	Dev% XCOM& Phy-x/PSD
NSZ1					
0.015	4.883			4.868	0.307
0.02	2.148			2.142	0.279
0.03	0.7521	0.752242	0.018863	0.750	0.279
0.04	0.4133	0.409112	-1.02365	0.412	0.315
0.05	0.2908	0.286263	-1.58479	0.290	0.275
0.06	0.2345	0.235012	0.217768	0.234	0.213
0.08	0.1851	0.184157	-0.51206	0.185	0.054
0.1	0.163	0.159971	-1.89335	0.163	0.000
0.15	0.1372	0.139355	1.546298	0.137	0.146
0.2	0.1232	0.122532	-0.54487	0.123	0.162
0.3	0.1058	0.103983	-1.74709	0.106	-0.189
0.356 (0.992)*	0.09889	0.097587	1.317304	0.099	-0.111
0.4	0.09436	0.092834	-1.6439	0.094	0.382
0.5	0.08601	0.084953	-1.24381	0.086	0.012
0.6	0.07948	0.080527	1.300022	0.079	0.604
0.662 (0.0751)*	0.07607	0.074814	-1.70496	0.076	0.092
0.8	0.06975	0.069411	-0.48902	0.070	-0.358
1	0.06268	0.063217	0.849061	0.063	-0.511
1.17 (0.0581)*	0.05796	0.058741	1.448174	0.058	-0.069
1.33 (0.0551)*	0.0543	0.053427	-1.54059	0.054	0.552
1.5	0.05104	0.05192	1.694252	0.051	0.078
2	0.04399	0.043523	-1.07242	0.044	-0.023
3	0.03575	0.035694	-0.15728	0.036	-0.699
4	0.0311	0.031627	1.664994	0.031	0.322
5	0.02813	0.028328	0.698531	0.028	0.462
6	0.0261	0.025858	-0.93734	0.026	0.383
8	0.02356	0.023493	-0.28413	0.024	-1.868
10	0.0221	0.021738	-1.6641	0.022	0.452
15	0.02038	0.020621	1.167737	0.020	1.865
NSZ2					
0.015	5.527			6.152	-11.308
0.02	4.712			7.083	-50.318
0.03	1.633	1.603237	-1.85642	2.448	-49.908
0.04	0.8149	0.823615	1.058181	1.186	-45.539
0.05	0.5062	0.513986	1.514879	0.705	-39.273
0.06	0.3629	0.359654	-0.90261	0.482	-32.819
0.08	0.2413	0.243578	0.935118	0.293	-21.426
0.1	0.1924	0.190222	-1.14513	0.220	-14.345
0.15	0.146	0.146664	0.452543	0.154	-5.479
0.2	0.1268	0.128932	1.653542	0.130	-2.524
0.3	0.1066	0.107872	1.179072	0.108	-1.313
0.356(0.0974)*	0.09931	0.0995	0.172284	0.100	-0.695
0.4	0.09458	0.093842	-0.78628	0.095	-0.444
0.5	0.086	0.085655	-0.40243	0.086	0.000
0.6	0.07936	0.078544	-1.03948	0.079	0.454
0.662 (0.0749)*	0.07592	0.0758	-0.17797	0.076	-0.105
0.8	0.06956	0.068492	-1.55964	0.069	0.805
1	0.06248	0.062233	-0.3962	0.062	0.768
1.77 (0.0587)*	0.05775	0.0565	-2.04805	0.058	-0.433
1.33 (0.0549)*	0.0541	0.053	-2.00699	0.054	0.185
1.5	0.05086	0.050803	-0.11236	0.051	-0.275
2	0.04387	0.043902	0.072636	0.044	-0.296
3	0.03575	0.035356	-1.11336	0.036	-0.699
4	0.03119	0.031517	1.036132	0.031	0.609
5	0.02831	0.028189	-0.42881	0.028	1.095

Table 5 (continued)

Energy	MAC from XCOM	MAC from MCNP5	Dev% XCOM&MCNP	MAC from Phy-x/PSD	Dev% XCOM& Phy-x/PSD
6	0.02635	0.026559	0.785184	0.027	-2.467
8	0.02393	0.023839	-0.38044	0.024	-0.293
10	0.02256	0.022844	1.24519	0.023	-1.950
15	0.021	0.021408	1.905751	0.022	-4.762
NSZ3					
0.015	6.172	-2.49529		7.316	-18.535
0.02	7.275	-1.20896		11.560	-58.900
0.03	2.514	2.5	-0.74966	3.986	-58.552
0.04	1.216	1.21	-0.58231	1.887	-55.181
0.05	0.7215	0.729	0.983197	1.081	-49.827
0.06	0.4914	0.485	-1.22912	0.706	-43.671
0.08	0.2975	0.3	0.678965	0.391	-31.429
0.1	0.2217	0.219	-1.27426	0.271	-22.237
0.15	0.1548	0.156	0.905477	0.170	-9.819
0.2	0.1304	0.129	-1.18903	0.137	-5.061
0.3	0.1075	0.109	1.463758	0.109	-1.395
0.356 (0.0992)*	0.09973	0.0101	1.695848	0.101	-1.273
0.4	0.0948	0.0953	0.507122	0.095	-0.211
0.5	0.08598	0.085	-1.11685	0.086	-0.023
0.6	0.07924	0.0787	-0.65137	0.079	0.303
0.662 (0.0762)*	0.07576	0.0775	2.184785	0.076	-0.317
0.8	0.06937	0.0701	1.074753	0.069	0.533
1	0.06227	0.0617	-1.00422	0.062	0.434
1.77 (0.0566)*	0.05755	0.0573	-0.34966	0.057	0.956
1.33 (0.0540)*	0.05391	0.0541	0.362019	0.054	-0.167
1.5	0.05068	0.0501	-1.24731	0.050	1.342
2	0.04374	0.0438	0.168025	0.044	-0.594
3	0.03575	0.0355	-0.67532	0.036	-0.699
4	0.03129	0.0319	1.857337	0.031	0.927
5	0.02849	0.0281	-1.56366	0.029	-1.790
6	0.0266	0.0269	1.041456	0.027	-1.504
8	0.02429	0.0242	-0.47194	0.025	-2.923
10	0.02301	0.0231	0.398507	0.024	-4.302
15	0.02162	0.0217	0.357912	0.023	-6.383
NSZ4					
0.015	7.462			9.344	-25.221
0.02	12.4			19.363	-56.153
0.03	4.277	4.256724	-0.47633	6.668	-55.904
0.04	2.02	1.991094	-1.45177	3.109	-53.911
0.05	1.152	1.143014	-0.78618	1.736	-50.694
0.06	0.7484	0.755215	0.902351	1.097	-46.579
0.08	0.4099	0.411726	0.443449	0.563	-37.351
0.1	0.2804	0.275263	-1.86612	0.360	-28.388
0.15	0.1723	0.170312	-1.16736	0.196	-13.755
0.2	0.1376	0.139731	1.524994	0.148	-7.558
0.3	0.1093	0.107795	-1.39624	0.112	-2.470
0.356 (0.102)*	0.1006	0.10186	1.23716	0.102	-1.392
0.4	0.09523	0.094225	-1.06713	0.096	-0.809
0.5	0.08594	0.087404	1.674855	0.086	-0.070
0.6	0.079	0.079584	0.733652	0.079	0.000
0.662 (0.0759)*	0.07546	0.0744	-1.46664	0.075	0.610
0.8	0.06899	0.068592	-0.58052	0.069	-0.014
1	0.06186	0.061343	-0.84304	0.061	1.390
1.17 (0.0562)*	0.05714	0.0567	-0.73701	0.057	0.245
1.33 (0.0542)*	0.05352	0.0532	-0.50412	0.053	0.972
1.5	0.05033	0.049835	-0.99411	0.050	0.656

Table 5 (continued)

Energy	MAC from XCOM	MAC from MCNP5	Dev% XCOM&MCNP	MAC from Phy-x/PSD	Dev% XCOM& Phy-x/PSD
2	0.0435	0.044339	1.89293	0.043	1.149
3	0.03575	0.035201	-1.55878	0.036	-0.699
4	0.03148	0.031064	-1.33925	0.032	-1.652
5	0.02885	0.028729	-0.42068	0.029	-0.520
6	0.0271	0.026916	-0.6837	0.028	-3.321
8	0.02502	0.025148	0.507931	0.026	-3.917
10	0.02392	0.023727	-0.81394	0.025	-4.515
15	0.02287	0.022733	-0.6014	0.025	-9.314

*Represents the experimental measured value of MAC

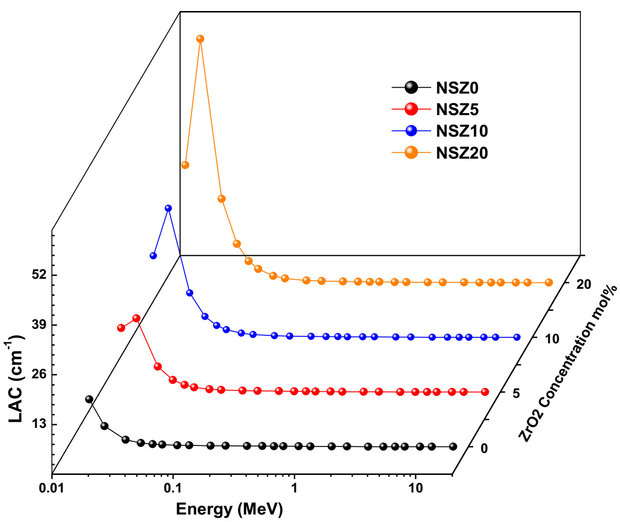

Fig. 7 Variation of LAC versus energy at different concentration of zirconium oxide

(5.4, 19.33, 33.75 and 63.7) cm^{-1} for NSZ1, NSZ2, NSZ3 and NSZ4 samples, then decrease to (0.052, 0.059, 0.066 and 0.081) at higher energy [42–46]. ZrO_2 plays a significant role in improving LAC. As a result, as ZrO_2 concentration rises, LAC rises as well, because ZrO_2 has high molecular weight than SiO_2. Mean free path (MFP) [47] of NSZ glasses are illustrated in Fig. 8. MFP values dramatically decrease as ZrO_2 increases, as shown in Fig. 8. The results show that NSZ glasses have lower MFP values than conventional concrete, 100% SiO_2, and 100% $Na_2B_4O_7$. Figure 9a, shows the "half-value length" HVL of NSZ glasses. The HVL values at all energies decline as ZrO_2 is increased. As illustrated in Fig. 9b and Table 6 [48]. The decreasing line of HVL values for $50Na_2O$-(50—x) SiO_2 – x ZrO_2 glasses are due to the increasing in MAC and density.

Fig. 8 Variation MFP with the photon energy for NSZ glasses and SiO_2 and $Na_2B_4O_7$ glasses

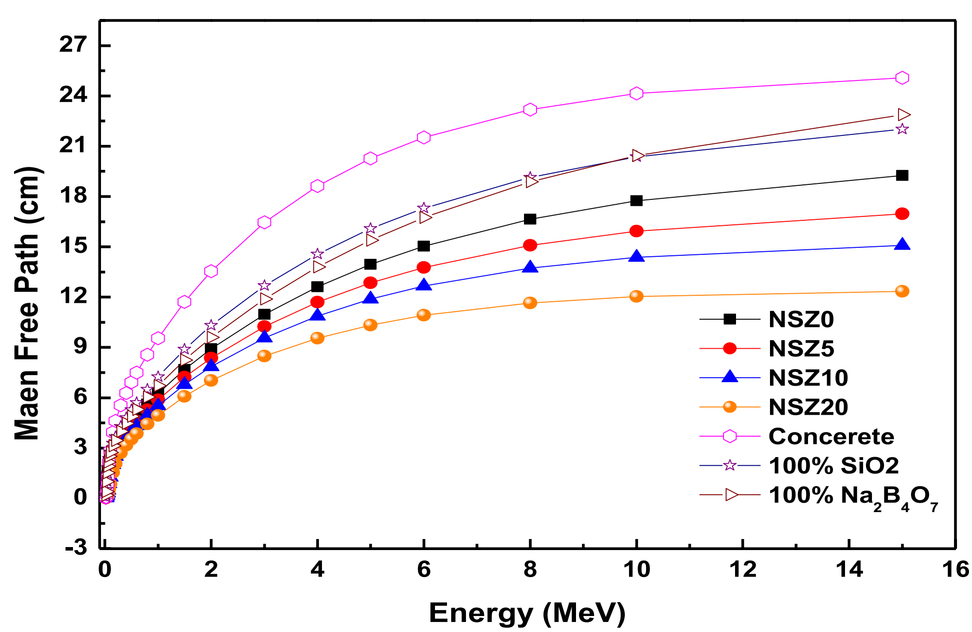

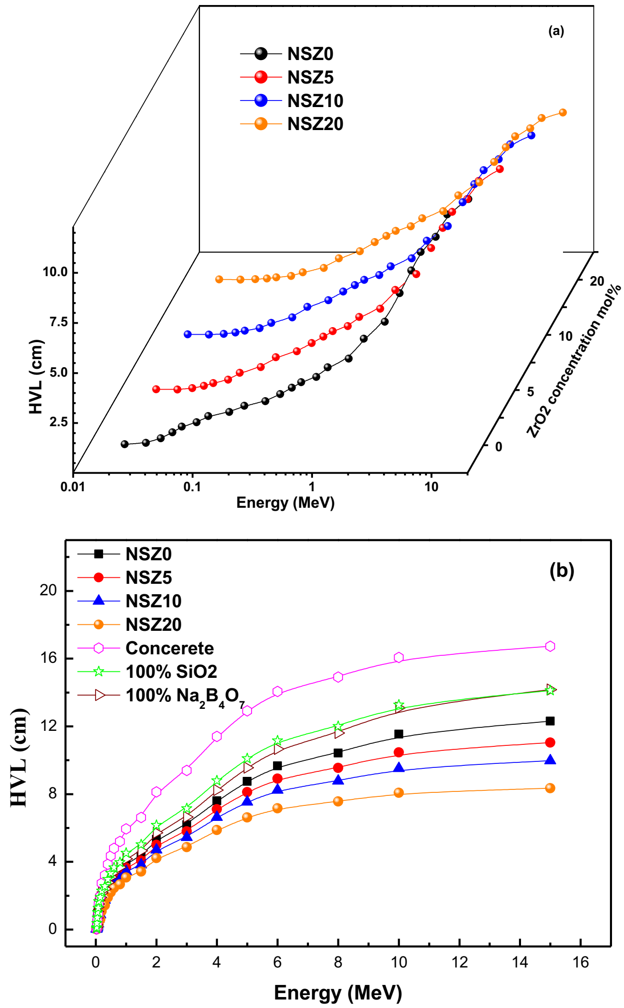

Fig. 9 Variation of HVL versus energy at different concentration of zirconium oxide (**a**) and with a comparison of other glasses (**b**)

HVL of NSZ samples is lower than that of concrete and other glasses.

Z_{eff} "effective atomic number" of NSZ samples is depicted in Fig. 10a. Because of the photoelectric effect, it has a higher value at low energy and the curvature shows that Z_{eff} declines faster in the energy range (0.04 -1.5 MeV). After 1.5 MeV, the value of Z_{eff} begins to rise, indicating that the shielding strength radiation is improved. Also, the N_{eff} "effective electron number" is depicted in Fig. 10b. It was observed that N_{eff} is strongly linked to Z_{eff}. Z_{eq} of NSZ glass system displayed in Fig. 10c. A qualitative examination on this figure reveals that the variation of N_{eff} by photon energy can be explained using the same way that was followed for Z_{eff}. Hence, the variations of N_{eff} values through the entire energy range can be explained by depending on the main photon interactions with glass materials and the chemical contents of the glass systems. The Z_{eq} value for the NSZ20 sample is greater than the other.

Figures 11 and 12 illustrate the calculated EBF& EABF "exposure buildup factors & energy absorption buildup factors" values for the NSZ glass system. For NSZ glasses, Due to the PE processes, the EBF and EABF values of glasses are minimum in the low energy. Whereas, at intermediate energy region, the EBF and EABF values of glasses raise up to the maximum as the energy increases. This behavior may be ascribed to multiple scattering by CF. At higher energy, there is an growth in the EABF values that is associated to the pair production process [49, 50]. EBF and EABF values for all glass samples at 0.015, 1.5, and 15 MeV, based on the depth of penetration, are shown in Fig. 13. The highest value of EBF and EABF is observed in NSZ1, and the lowest value is observed in NSZ4.

Table 6 Comparison of MAC (cm^2/g) and HVL (cm)of NSZ glass with other published materials [59]

Samples and concrete	MAC (cm^2/g)		HVL cm		
	662 keV	1173 keV	662 keV	1173 keV	1332 keV
NSZ1	0.0752	0.0582	3.574	4.697	5.013
NSZ2	0.0749	0.0587	3.348	4.414	4.711
NSZ3	0.0763	0.0566	3.139	4.149	4.429
NSZ4	0.0759	0.0571	2.799	3.718	3.970
Ordinary	0.0778	0.0592	3.87	5.-9	5.43
Barite	0.0780	0.0565	2.54	3.5	3.75
Ferrite	0.0777	0.0589	1.98	2.62	2.79
Chromate	0.0751	0.0569	2.82	3.72	3.97
Serpentite	0.0779	0.0592	4.07	6.00	6.40

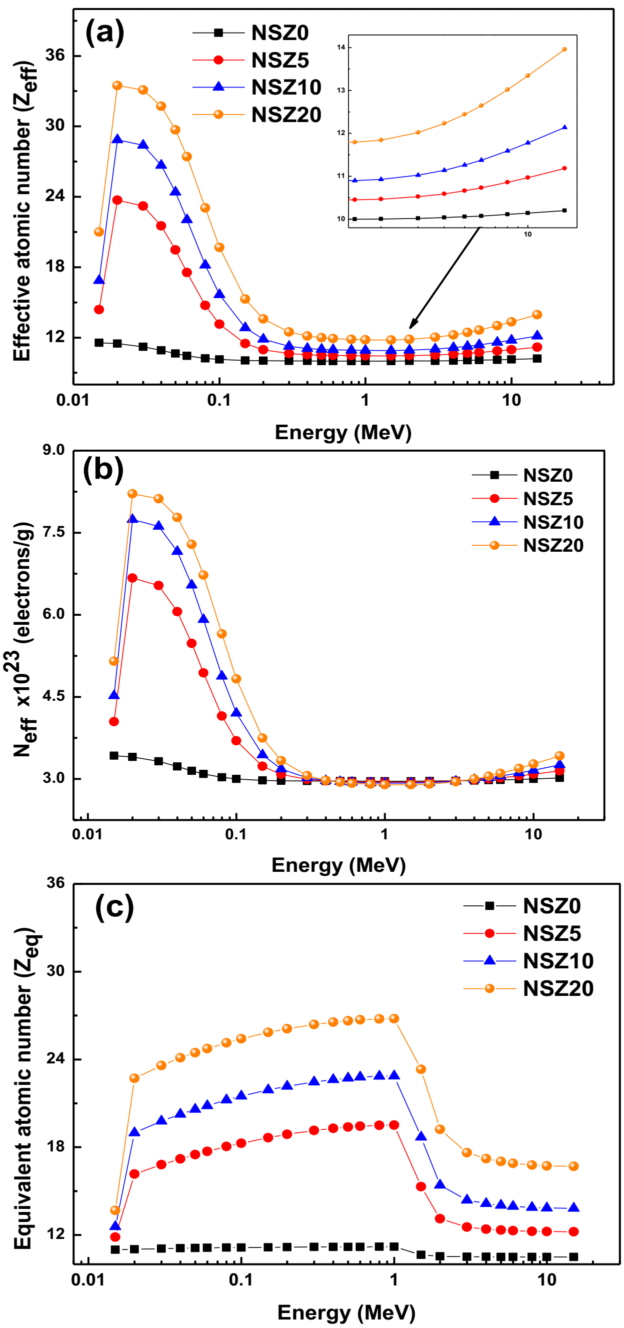

Fig. 10 The Z_{eff} (**a**), N_{eff}(**b**) and Z_{eq}(**c**) gamma photons energy for NSZ glasses

The efficiency of radiation protection (RP) is described as [51]:

$$RP = (1 - \frac{I}{I_o}) \times 100 \quad (13)$$

The *RP* was calculated by Eq. 13 and mentioned in Table 7 for NSZ glasses. It was found that the NSZ4 sample has *RP* 30.42% and 17.82% at 356 keV and 1332 keV respectively, it proves more effective. Table 7 also, shows a comparison between the MAC data measured experimentally at photon energy 356, 662, 1172 and 1332 keV and those calculated from the different computer programs. It is seen that good agreement was detected.

ΣR "Fast neutrons removal cross-sections" of fabricated samples are demonstrated in Fig. 14. It was found ΣR of NSZ samples are 0.091, 0.094, 0.097, and 0.102 (1/cm) for NSZ1, NSZ2, NSZ3, and NSZ4. With the addition of zirconium oxide, ΣR gradually increases. This rise is due to the replacement of Zr which has a higher atomic number at the expense of Si and O. Figure 14 shows a comparison of the current NSZ glasses with shielding concrete. The NSZ4 sample was discovered to be a promising shielding glass.

4 Conclusions

Crystallization and radiation shielding features of ternary glasses Na_2O-SiO_2-ZrO_2 containing various molar fractions of ZrO_2 have been evaluated in the current paper. ZrO_2/SiO_2 replacement improves the connectivity of the glass matrix. Therefore, T_g, T_c, and T_p values are increased by an increment of ZrO_2. It indicated that these increasing with an increase of ZrO_2 content due to the formation of strong bond Si − O − Zr. The XRD results for heat-treated glasses show that most glasses appear to be completely crystallized. Particularly, as ZrO_2 increments, the intensity increases, and the peak position is slightly shifted towards higher 2θ° values. The character of ZrO_2 on gamma-ray shielding characteristics of SiO_2- Na_2O-ZrO_2 samples are evaluated experimentally and by using computer programs XCOM, MCNP and Phy-X/PSD. The inclusion of ZrO_2 to the glasses shield has been shown to enhance the MAC. With comparison, it was recognized the presence of ZrO_2 supports to raise MAC and μ_m. When the MFP values of glasses are compared to the MFP values of commercial glasses such as borax and quartz, it becomes clear that our glasses have superior shielding capabilities. Many concrete, including Ordinary, Barite, Ferrite, Chromate, and Serpentine, have a lower HVL value than NSZ glasses. NSZ samples have the smallest EBF and EABF values at the highest ZrO_2. (ΣR) calculations indicated the capability of the NSZ samples for neutron attenuation.

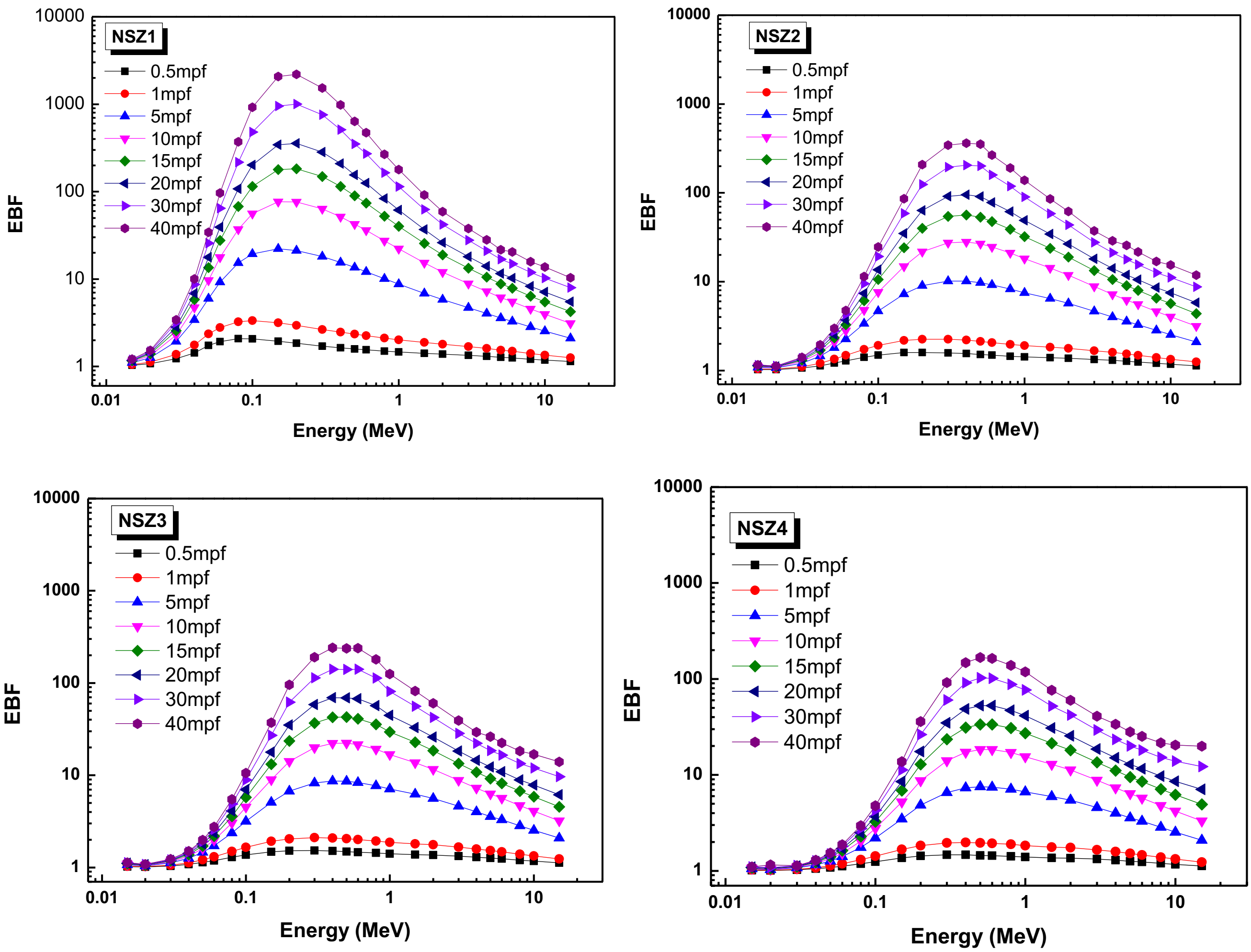

Fig. 11 The variation of EBF for NSZ glasses versus gamma energies

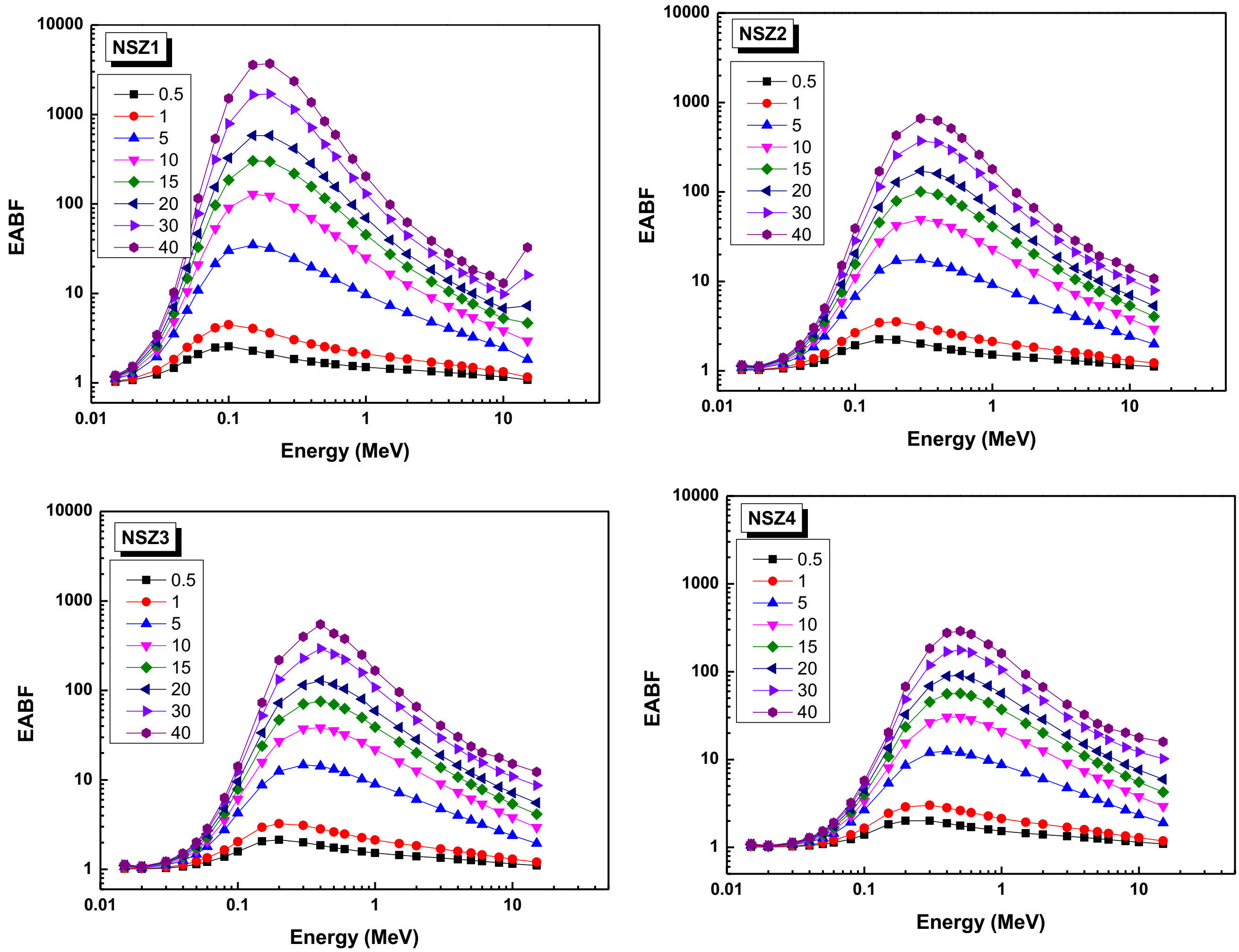

Fig. 12 The variation of EABF for NSZ glasses versus gamma energies

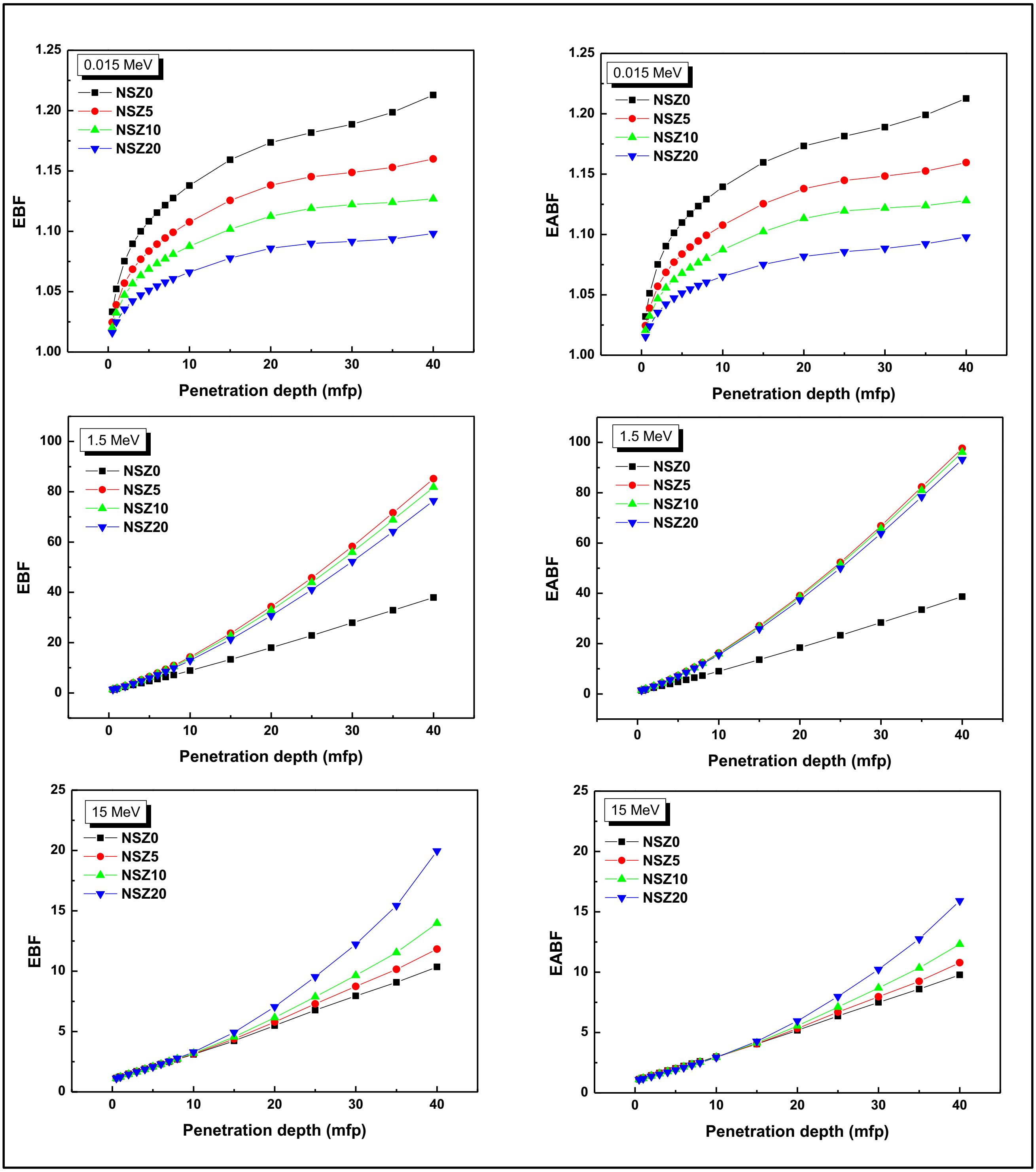

Fig. 13 The variation of EBF and EABF factors for NSZ glasses versus penetration depth

Table 7 Experimental and simulation MAC for NSZ glasses and its radiation protection efficiency

Samples	E keV	$\mu_m = \mu_L/\rho$			RD			Radiation protection efficiency
		Exp.* 10^{-2}	x.com* 10^{-2}	MCNP5*10^{-2}	$(RD^a)\times10^2$	$(RD^b)\times10^2$	$(RD^c)\times10^2$	$(1-(i/i_o))*100$
NSZ1	356	9.925	9.889	9.759	1.317	0.3635	-1.673	24.30049
	662	7.517	7.607	7.481	-1.705	-1.221	-0.4816	19.01105
	1173	5.816	5.796	5.874	1.448	0.4721	0.9893	15.05376
	1332	5.519	5.430	5.343	-1.541	1.710	-3.196	14.343
NSZ2	356	9.749	9.931	9.948	0.1722	-1.858	2.032	27.34185
	662	7.492	7.592	7.581	-0.1779	-1.358	1.185	21.76438
	1173	5.876	5.775	5.652	-2.048	1.845	-3.819	17.51152
	1332	5.497	5.410	5.299	-2.007	1.682	-3.610	16.48109
NSZ3	356	9.927	9.973	10.145	1.696	-0.4658	2.199	22.96229
	662	7.629	7.576	7.748	2.185	0.6624	1.553	18.1682
	1173	5.662	5.755	5.728	-0.3497	-1.525	1.172	13.82488
	1332	5.409	5.391	5.406	0.3620	0.4327	-0.063	13.25169
NSZ4	356	10.165	10.06	10.186	1.23716	1.029	-0.3314	30.77859
	662	7.5912	7.546	7.439	-1.467	0.5768	-2.012	24.02355
	1173	5.629	5.714	5.665	-0.7370	-1.369	0.6227	18.43318
	1332	5.422	5.352	5.32	-0.5041	1.385	-1.883	17.81739

RD^a = (MCNP5 -x.com)/ x.com. RD^b = (Exp-x.com)/Exp., RD^c = (Exp- MCNP5)/Exp
=

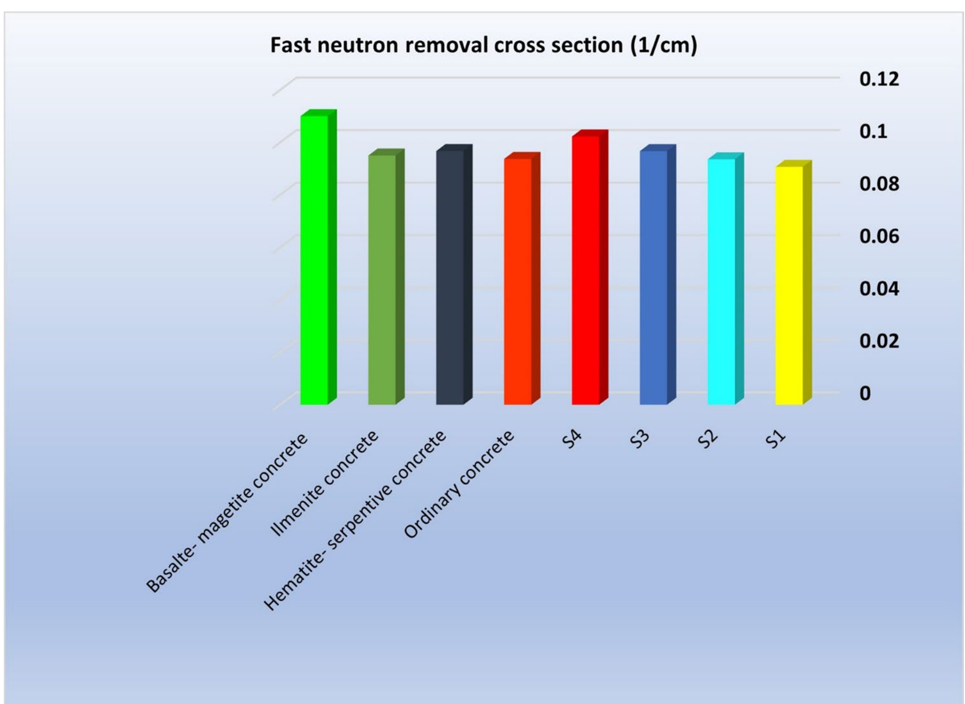

Fig. 14 FNRCS of NSZ glasses in comparison with other concrete shielding

Acknowledgements We would like to thank Taif University Research Supporting Project number (TURSP-2020/24), Taif University, Taif, Saudi Arabia. Moreover, the authors express their gratitude to the Deanship of Scientific Research at King Khalid University for funding this work through research groups program under grant number R.G.P. 2/137/42.

Author contributions Kh. S. Shaaban, Sayed A. Makhlouf, and E.A. Abdel Wahab Conceptualization, Methodology, Writing Reviewing Discussion. Ateyyah M. Al-Baradi, M. A. Sayed and Atif Mossad Ali: Writing Reviewing Discussion.

Funding There are currently no Funding Sources on the list.

Data availability My manuscript and associated personal data.

The manuscript has not been published.

Declarations

Conflict of Interest The authors declare that they have no conflict of interest.

Declaration of Competing Interest The authors declare that they have no known competing financial interests.

Consent to Participate The authors consent to participate.

Consent for Publication The author's consent for publication.

References

1. Abdel Wahab EA, Shaaban KS, Elsaman R et al (2019) Radiation shielding, and physical properties of lead borate glass doped ZrO_2 nanoparticles. Appl Phys A 125:869. https://doi.org/10.1007/s00339-019-3166-8
2. Chandrakala C, Reddy ASS, Jedryka J et al (2020) Third-order nonlinear optical features of zirconia-added lead silicate glass ceramics embedded with $Pb_2Fe_2O_5$ perovskite crystal phases and role of Fe ions. Appl Phys A 126:413. https://doi.org/10.1007/s00339-020-03570-x
3. Fisher JG, James PF, Parker JM (2005) Soda lime zirconia silicate glasses as prospective hosts for zirconia-containing radioactive wastes. J Non-Cryst Solids 351(8–9):623–631. https://doi.org/10.1016/j.jnoncrysol.2005.01.064
4. Loiseau P, Caurant D, Majerus O et al (2003) Crystallization study of (TiO_2, ZrO_2)-rich SiO_2-Al_2O_3-CaO glasses Part I Preparation and characterization of zirconolite-based glass-ceramics. J Mater Sci 38:843–852. https://doi.org/10.1023/A:1021873301498
5. Rao CS, Srikumar T, Gandhi Y, Ravikumar V, Veeraiah N (2011) Dielectric and spectroscopic investigations of lithium aluminium zirconium silicate glasses mixed with TiO_2. Phil Mag 91(6):958–980. https://doi.org/10.1080/14786435.2010.531056
6. Moustafa MG, Hassaan MY (2017) Optical and dielectric properties of transparent ZrO_2 –TiO_2 –$Li_2B_4O_7$ glass system. J Alloy Compd 710:312–322. https://doi.org/10.1016/j.jallcom.2017.03.192
7. Lu, X., Deng, L., Kerisit, S. et al. Structural role of ZrO_2 and its impact on properties of boroaluminosilicate nuclear waste glasses. npj Mater Degrad 2, 19 (2018). https://doi.org/10.1038/s41529-018-0041-6
8. St-Pierre J, Tran HH, Zikovsky L (1982) Immobilization of radioactive wastes: Leachability of glasses containing zirconium. J Nucl Mater 107(2–3):286–289. https://doi.org/10.1016/0022-3115(82)90427-5
9. Abdel Wahab, E.A., El-Maaref, A.A., Shaaban, K.S., Börcsök, J., Abdelawwad, M., 2021. Lithium cadmium phosphate glasses doped Sm3+ as a host material for near-IR laser applications, 111:110638. https://doi.org/10.1016/j.optmat.2020.110638
10. Shaaban KS, Yousef ES, Mahmoud SA et al (2020) Mechanical, Structural and Crystallization Properties in Titanate Doped Phosphate Glasses. J Inorg Organomet Polym 30:4655–4663. https://doi.org/10.1007/s10904-020-01574-x
11. Wahab EAA, Shaaban KS, Al-Baradi AM (2021) Enhancement of Optical and Physical Parameters of Lead Zinc Silicate Glasses by Doping W+3 Ions. SILICON. https://doi.org/10.1007/s12633-021-01236-8
12. Abdel Wahab EA, Shaaban KhS (2021) Structural and optical features of aluminum lead borate glass doped with Fe_2O_3. Appl Phys A 127:956. https://doi.org/10.1007/s00339-021-05062-y
13. Connelly, A. J., Travis, K. P., Hand, R. J., Hyatt, N. C. & Maddrell, E. Composition-structure relationships in simplified nuclear waste glasses: 2. the effect of ZrO_2 additions. J. Am. Ceram. Soc. 94, 137–144 (2011). https://doi.org/10.1111/j.1551-2916.2010.04036.x
14. Shaaban KS, Zahran HY, Yahia IS et al (2020) Mechanical and radiation-shielding properties of B_2O_3–P_2O_5–Li_2O–MoO_3 glasses. Appl Phys A 126:804. https://doi.org/10.1007/s00339-020-03982-9
15. Bergeron B et al (2010) First investigations of the influence of IVB elements (Ti, Zr, and Hf) on the chemical durability of soda-lime borosilicate glasses. J Non Cryst Solids 356:2315–2322. https://doi.org/10.1016/j.jnoncrysol.2010.07.065
16. Fisher JG, James PF, Parker JM (2005) Soda lime zirconia silicate glasses as prospective hosts for zirconia-containing radioactive wastes. J Non Cryst Solids 351:623–631. https://doi.org/10.1016/j.jnoncrysol.2005.01.064
17. Abouhaswa AS, Al-Buriahi MS, Chalermpon M et al (2020) Influence of ZrO_2 on gamma shielding properties of lead borate glasses. Appl Phys A 126:78. https://doi.org/10.1007/s00339-019-3264-7
18. Li B, Li W, Zheng J (2018) Influence of Y_2O_3 Addition on Crystallization, Thermal, Mechanical, and Electrical Properties of BaO-Al_2O_3-B_2O_3-SiO_2 Glass-Ceramic for Ceramic Ball Grid Array Package. Journal of Elec Materi 47:766–772. https://doi.org/10.1007/s11664-017-5808-y
19. Danewalia SS, Khan S, Dhillon S et al (2020) Effect of transition metals (MO-TiO_2, MnO_2, Fe_2O_3, and ZnO) on crystallization and electrical conductivity of SiO_2–CaO–Na_2O–P_2O_5-based glass-ceramics. Ionics 26:2959–2967. https://doi.org/10.1007/s11581-019-03311-y
20. Sharma G, Arya SK, Singh K (2018) Optical and thermal properties of glasses and glass-ceramics derived from agricultural wastes. Ceram Int 44(1):947–952. https://doi.org/10.1016/j.ceramint.2017.10.027
21. Abdel Wahab, E.A., Shaaban, K.S. & Yousef, E.S. Enhancement of optical and mechanical properties of sodium silicate glasses using zirconia. Opt Quant Electron 52, 458 (2020). https://doi.org/10.1007/s11082-020-02575-3
22. Abdel Wahab, E. A., Aboraia, A. M., El Shafey, A. M., Shaaban, Kh. S., Soldatov, A. V. The effect of ZrO_2 on the linear and nonlinear optical properties of sodium silicate glass. Opt Quant Electron 53, 504 (2021). https://doi.org/10.1007/s11082-021-03164-8
23. Berger MJ, Hubbell JH, Seltzer SM, Chang J, Coursey JS, Sukumar R (1998) XCOM: photon cross sections database
24. Şakar E, Özpolat ÖF, Alım B, Sayyed MI, Kurudirek M (2019) Phy-X / PSD: Development of a user-friendly online software for calculation of parameters relevant to radiation shielding and

dosimetry. Radiat Phys Chem 108496. https://doi.org/10.1016/j.radphyschem.2019.108496
25. Hubbell JH (1982) Photon mass attenuation and energy-absorption. Int J Appl Radiat Isot 33:1269–1290
26. Pawar PP, Bichile GK (2013) Studies on mass attenuation coefficient, Zeff and electron density of some amino acids in the energy range 0.122-1.330 MeV. Radiat Phys Chem 92:22–27
27. Gaikwad DK, Pawar PP, Selvam TP (2017) Mass attenuation coefficients and effective atomic numbers of biological compounds for gamma ray interactions. Radiat Phys Chem 138:75–80. https://doi.org/10.1016/j.radphyschem.2017.03.040
28. Rammah YS, El-Agawany FI, El-Mesady IA (2019) Evaluation of photon attenuation and optical characterizations of bismuth lead borate glasses modified by TiO_2. Appl Phys Mater Sci Process 125. https://doi.org/10.1007/s00339-019-3023-9
29. Rammah YS, Sayyed MI, Abohaswa AS et al (2018) FTIR, electronic polarizability and shielding parameters of B_2O_3 glasses doped with SnO_2. Appl Phys A 124:650. https://doi.org/10.1007/s00339-018-2069-4
30. Jackson DF, Hawkes DJ (1981) X-ray attenuation coefficients of elements and mixtures. Phys Rep 70:169–233
31. Hine GJ (1952) The effective atomic numbers of materials for various gamma interactions. Phys Rev 85:725–737
32. Abdel Wahab EA, Koubisy MSI, Sayyed MI, Mahmoud KA, Zatsepin AF, Makhlouf SA, Shaaban KhS (2020) Novel borosilicate glass system: $Na_2B_4O_7$-SiO_2-MnO_2: Synthesis, average electronics polarizability, optical basicity, and gamma-ray shielding features. J Non-Cryst Solids 120509. https://doi.org/10.1016/j.jnoncrysol.2020.120509
33. Sardari D, Kurudriek M (2013) Studies on energy absorption and exposure buildup factors in some solutions of alkali metal chlorides. Int J Phys Sci 8(12):481–491
34. Wood JI (1982) Computational Methods in Reactor Shielding. Pergamon Press. Yalcin, Z., Icelli, O., Okutan, M., Boncukcuoglu, R., Artun, O., Orak, S., 2012. A different perspective to the effective atomic number ($Z_{(eff)}$) for some boron compounds and trommel sieve waste (TSW) with a new computer program ZXCOM. Nucl Instrum Methods A 686:43–47
35. Chilton AB Faw RE, Shultis JK (1984) Principles of Radiation Shielding. PrenticeHall, Englewood Cliffs
36. Kaplan MF (1989) Concrete Radiation Shielding: Nuclear Physics, Concrete Properties, Design and Construction. Longman Scientific & Technical
37. Lu X, Deng L, Kerisit S, Du J (2018) Structural role of ZrO_2 and its impact on properties of boroaluminosilicate nuclear waste glasses. Npj Mater Degrad 2(1). https://doi.org/10.1038/s41529-018-0041-6
38. Varshneya AK (1994) Fundamentals of inorganic glasses, Academic Prese Limited, 33
39. El-Rehim AFA, Shaaban KS, Zahran HY et al (2020) Structural and Mechanical Properties of Lithium Bismuth Borate Glasses Containing Molybdenum (LBBM) Together with their Glass-Ceramics. J Inorg Organomet Polym. https://doi.org/10.1007/s10904-020-01708-1
40. El-Rehim AFA, Zahran HY, Yahia IS et al (2020) Physical, Radiation Shielding and Crystallization Properties of Na_2O-Bi_2O_3-MoO_3-B_2O_3- SiO_2-Fe_2O_3 Glasses. SILICON. https://doi.org/10.1007/s12633-020-00827-1
41. El-Rehim AA, Zahran H, Yahia I et al (2020) Radiation, Crystallization, and Physical Properties of Cadmium Borate Glasses. SILICON. https://doi.org/10.1007/s12633-020-00798-3
42. Shaaban KHS, Saddeek YB, Aly KA et al (2019) Fabrication and Characterization of Glass and Glass-Ceramic from Cement Dust and Limestone Dust. SILICON 11:807–815. https://doi.org/10.1007/s12633-018-9964-3
43. Gurinder PS, Joga S, Parvinder K, Simranpreet K, Deepawali A, Ravneet K, Kulwinder K, Singh DP (2020) Analysis of enhancement in gamma ray shielding proficiency by adding WO_3 in Al_2O_3-PbO-B_2O_3 glasses using Phy-X/PSD. J Market Res 14425–14442. https://doi.org/10.1016/j.jmrt.2020.10.020
44. Dong MG, El-Mallawany R, Sayyed MI, Tekin HO (2017) Shielding properties of 80TeO_2–5TiO_2–(15–x) WO_3–xAnOm glasses using WinXCom and MCNP5 code. Radiat Phys Chem 141:172–178
45. Al-Hadeethi Y, Sayyed MI (2020) A comprehensive study on the effect of TeO_2 on the radiation shielding properties of TeO_2–B_2O_3–Bi_2O_3–LiF–$SrCl_2$ glass system using Phy-X/PSD software. Ceram Int 46:6136–6140
46. Şakar Erdem, Özpolat Özgür Fırat, BünyaminAlım MI, Sayyed Murat Kurudirek (2020) Phy-X/PSD: development of a user friendly online software for calculation of parameters relevant to radiation shielding and dosimetry. Rad Phys Chem. 166:108496
47. Singh KJ, Singh N, Kaundal RS, Singh K (2008) Gamma-ray shielding and structural properties of PbO–SiO_2 glasses. Nucl Instrum Methods Phys Res, Sect B 266(6):944–948. https://doi.org/10.1016/j.nimb.2008.02.004
48. Lakshminarayana G, Kumar A, Dong MG, Sayyed MI, Long NV, Mahdi MA (2018) Exploration of gamma radiation shielding features for titanate bismuth borotellurite glasses using relevant software program and Monte Carlo simulation code. J NonCryst Solids 481:65–73
49. Adem Un F (2013) Demir, Determination of mass attenuation coefficients, effective atomic numbers and effective electron numbers for heavy-weight and normal-weight concretes. Appl Radiat Isot 80:73–77
50. Mann HS, Brar GS, Mudahar GS (2016) Gamma ray shielding effectiveness of novel light weight clay flyash bricks. Radiat Phys Chem 127:97–101
51. Alomairy, S., Al-Buriahi, M.S., Abdel Wahab, E.A., Sriwunkum, C., Shaaban, K. 2021. Synthesis, FTIR, and neutron/charged particle transmission properties of Pb3O4–SiO2–ZnO–WO3 glass system. 47(12):17322–17330. https://doi.org/10.1016/j.ceramint.2021.03.045